Synthesis of NBN-type Zigzag-Edged Polycyclic Aromatic Hydrocarbons: 1,9-Diaza-9*a*-boraphenalene as a Structural Motif

Xinyang Wang,[†] Fan Zhang,[*,†] Karl Sebastian Schellhammer,[‡,§] Peter Machata,[#] Frank Ortmann,[‡] Gianaurelio Cuniberti,[‡,§] Yubin Fu,[§] Jens Hunger,[§] Ruizhi Tang,[†] Alexey A. Popov,[#] Reinhard Berger,[§] Klaus Müllen,[∥] and Xinliang Feng[*,†,§]

[†]School of Chemistry and Chemical Engineering, State Key Laboratory of Metal Matrix Composites, Shanghai Jiao Tong University, Shanghai 200240, P. R. China

[‡]Institute for Materials Science, Max Bergmann Center of Biomaterials and Dresden Center for Computational Materials Science, Technische Universität Dresden, 01062 Dresden, Germany

[§]Center for Advancing Electronics Dresden (cfaed) & Department of Chemistry and Food Chemistry, Technische Universität Dresden, 01062 Dresden, Germany

[#]Center of Spectroelectrochemistry, Department of Electrochemistry and Conducting Polymers, Leibniz Institute for Solid State and Materials Research, 01069 Dresden, Germany

[∥]Max Planck Institute for Polymer Research, Ackermannweg 10, 55128 Mainz, Germany

ABSTRACT: A novel class of dibenzo-fused 1,9-diaza-9*a*-boraphenalenes featuring zigzag edges with a nitrogen-boron-nitrogen bonding pattern named NBN-dibenzophenalenes (NBN-DBPs) has been synthesized. Alternating nitrogen and boron atoms imparts high chemical stability to these zigzag-edged polycyclic aromatic hydrocarbons (PAHs), this motif even allows for post-synthetic modifications, as demonstrated here through electrophilic bromination and subsequent palladium-catalyzed cross-coupling reactions. Upon oxidation, as a typical example, NBN-DBP **5a** was nearly quantitatively converted to σ-dimer **5a-2** through an open-shell intermediate, as indicated by UV-vis-NIR absorption spectroscopy and electron paramagnetic resonance (EPR) corroborated by spectroscopic calculations, as well as 2D NMR spectra analyses. *In-situ* spectroelectrochemistry was used to confirm the formation process of the dimer radical cation **5a-2**$^{\cdot+}$. Finally, the developed new synthetic strategy could also be applied to obtain π-extended NBN-dibenzoheptazethrene (NBN-DBHZ), representing an efficient pathway towards NBN-doped zigzag-edged graphene nanoribbons.

INTRODUCTION

Phenalene (**1**) is the smallest D_{3h}-symmetric polycyclic aromatic hydrocarbon (PAH) with thirteen carbon atoms and thirteen π-electrons. Thus one electron remains unpaired, rendering this PAH with an open shell character (Figure 1). Moreover, this compound is a structural motif of nanographenes and graphene nanoribbons (GNRs) that are terminated exclusively by zigzag-edged peripheries.[1] The neutral form of phenalene is a resonance-stabilized radical that can be generated and observed at room temperature in solution,[2] but the study of its optoelectronic properties remains difficult.[3] Implementation of heteroatoms into the phenalene backbone can strongly influence the chemical and physical properties, as exampled by 1-azaphenalene (**2**)[4] or 9*b*-boraphenalene (**3**).[5] Furthermore, introduction of bilateral benzenes rings has been widely used for phenalene derivatives to induce steric shielding of the highly reactive periphery and thus increases the kinetic stability.[6] We have recently reported that 9*a*-azaphenalene, which contains a nitrogen atom as a bridgehead within the zigzag-edged periphery, exhibiting a stabilized zwitterionic structure similar to an azomethine ylide (AMY) with high chemical reactivity.[7]

The implementation of combinations of heteroatoms, such as nitrogen and boron, for example substituting a C=C unit in aromatic molecules with an isoelectronic B-N moiety could significantly affect the electronic structures while leaving the conjugated skeleton unchanged.[8] In addition, the B-N bond other than the nonpolar C=C bond, could also be considered as a zwitterionic double bond in the neutral state and the oxidation process of the B-N bond has recently received growing interest because of the potential physicochemical properties based on the Lewis acid or base properties of these heteroatoms.[9]

More recently, different from usually only two carbon atoms that are replaced by heteroatoms,[10] replacement of a full C3-Unit of the zigzag edge with heteroatoms raised the interest, allowing the synthesis of stable PAHs with extended zigzag-edges: For example, oxygen-boron-oxygen (OBO)-doped double [5]helicenes with substantial

chemical and thermal stabilities were synthesized by Hatakeyama's group, showing excellent ambipolar conductivity.[11] At the same time, our group successfully prepared OBO-doped peritetracenes via the cyclodehydrogenation of OBO-doped double [5]helicenes,[12] offering the possibility for the construction of novel heteroatom-doped nanographenes.[13]

In addition to the incorporation of OBO-doped structure, the nitrogen-boron-nitrogen (NBN) containing aromatic molecules have also raised interests in molecular optoelectronic materials, while the NBN units are in most restricted in one fused ring.[14] During the preparation of our manuscript, the first example of NBN incorporated organic-inorganic hybrid polymer was reported by Helten's group, and introduction into a PAH with limited π-conjugation across the NBN unit was proved.[15]

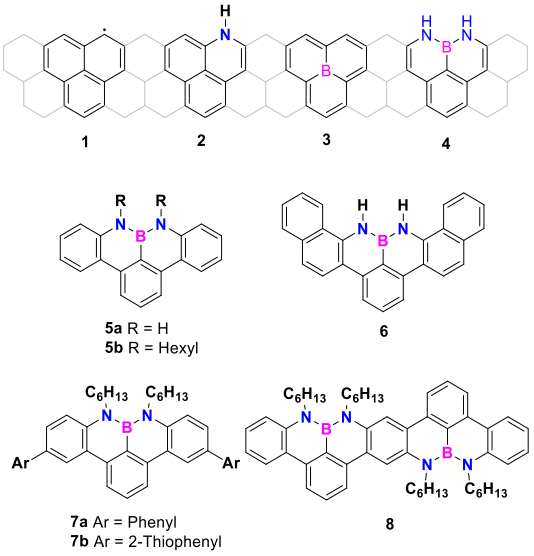

Figure 1. Phenalene (**1**), 1-azaphenalene (**2**), 9*b*-boraphenalene (**3**) and the unprecedented 1,9-diaza-9*a*-boraphenalene (**4**). Newly synthesized benzo-elongated (**5a-b**), π-extended (**6**) and aryl substituted (**7a-b**) derivatives, as well as the higher homologue **8**.

Herein, our efforts to understand the effects of heteroatom doping at the zigzag edges of phenalenyl systems on the stability and optoelectronic properties have focused on exploring N-B-N incorporated heterophenalenes based on a 1,9-diaza-9*a*-boraphenalene (**4**) core motif, in particular, NBN-doped benzo-elongated phenalene structures (**5** - **8**) were first reported.[16] Besides, one-electron oxidation of the 4π-electron N-B-N unit could lead to the 3π-electron (N-B-N)* unit, which is isoelectronic to the allylic C-C-C unit, thereby making the open shell odd-electron π systems, leading to isoelectronic derivatives of the else unprecedented full-carbon dibenzophenalenyl radical.

RESULTS AND DISCUSSION

In this work, the syntheses of benzo-elongated zigzag-edged 8*H*,9*H*-8,9-diaza-8a-borabenzo[*fg*]tetracene (**5a**) and its alkylated derivative 8,9-dihexyl-8*H*,9*H*-8,9-diaza-8a-borabenzo[*fg*]tetracene (**5b**) (or dibenzo-fused 1,9-diaza-9a-diboraphenalenes, denoted as NBN-DBP) were established and further extended to 10,11-dihydro-10,11-diaza-10a-boratribenzo[*a,fg,l*]tetracene (**6**). The high chemical stability of the N-B-N zigzag–edged NBN-DBPs allows for an electrophilic bromination process and subsequent derivatization by palladium-catalyzed cross-couplings, as exemplified by 8,9-dihexyl-5,12-diphenyl-8*H*,9*H*-8,9-diaza-8a-borabenzo[*fg*]tetracene (**7a**) and 8,9-dihexyl-5,12-(2-thienyl)-8*H*,9*H*-8,9-diaza-8a-borabenzo[*fg*]tetracene (**7b**). Moreover, 8,9,18,19-tetrahexyl-*8H,9H,18H,19H*-8,9,18,19-tetraaza-8a,18a-diboradibenzo[a,b,,lm]heptacene (**8**), which is the next homologue and a diazabora-derivative of dibenzoheptazethrene (denoted as NBN-DBHZ), was synthesized to highlight the scope of this solution-based approach toward elongated NBN-edged PAHs. Single-crystal X-ray analyses of compounds **5b**, **6**, **7a** and **13** demonstrated that the BN bonds have double-bond character. Theoretical, spectroscopic, and electrochemical studies revealed the aromaticity and optoelectronic properties of these unprecedented NBN-edged PAHs. Upon chemical oxidation, as an example, NBN-DBP **5a** was nearly quantitatively converted to σ-dimer **5a-2** through an open-shell intermediate, as indicated by UV-vis-NIR absorption spectroscopy and electron paramagnetic resonance (EPR) corroborated by spectroscopic calculations. The chemical structure of **5a-2** was unambiguously confirmed by 2D-NMR analysis and MALDI-TOF MS as N-*para* C-C coupling dimer. To get insight into the radical cation of the NBN-DBP after single-electron oxidation, we performed *in-situ* spectroelectrochemical studies of **7a**. The diphenyl substituents at the N-*para* positions of the NBN-DBP successfully prevented oligomerization and allowed *in-situ* VIS-NIR and EPR characterizations of the open shell radical cation $\mathbf{7a}^{\cdot+}$. For $\mathbf{7a}^{\cdot+}$ a large bathochromic shift up with maximum absorption at 1384 nm was observed together with a broad EPR signal at g = 2.0026 and a homogenous spin-density distribution over the whole PAH framework.

Scheme 1. Synthesis of NBN-dibenzophenalene (NBN-DBP) derivatives.

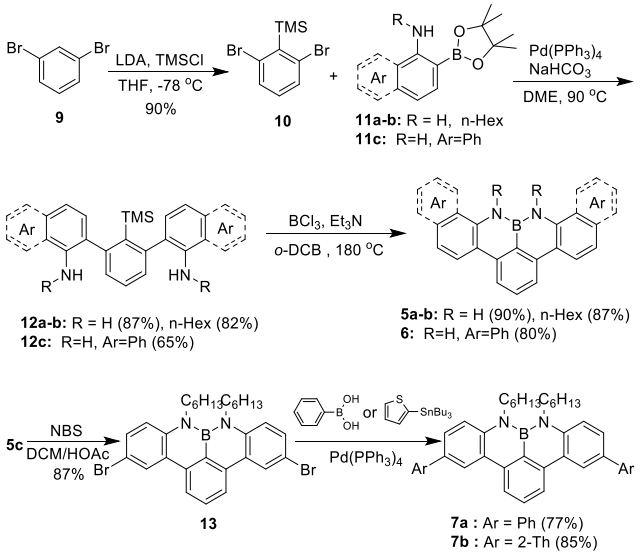

Synthesis and Structural Characterization. The targeted NBN-DBP derivatives **5a-b** and **6** were synthesized in three steps, as depicted in Scheme 1. A trimethylsilyl (TMS) group was introduced to act as a directing group during facile twofold electrophilic aromatic borylation, which was used to fuse the N-B-N unit at the perimeter of the PAH in high yield.[17] First, 1,3-dibromobenzene (**9**) was selectively lithiated in the 2-position using lithium diisopropyl amide (LDA), and this reaction was quenched with trimethylsilyl chloride to provide 1,3-dibromo-2-(trimethylsilyl)benzene (**10**) in 90% yield.[18] In the second step, palladium-catalyzed Suzuki couplings of **10** with the respective 2-amino boronic acid esters, 2-(4,4,5,5-tetramethyl-1,3,2-dioxaborolan-2-yl)aniline (**11a**), *N*-hexyl-2-(4,4,5,5-tetramethyl-1,3,2-dioxaborolan-2-yl)aniline (**11b**) or 2-(4,4,5,5-tetramethyl-1,3,2-dioxaborolan-2-yl)naphthalen-1-amine (**11c**) provided uncyclized intermediates 2'-(trimethylsilyl)-[1,1':3',1''-terphenyl]-2,2''-diamine (**12a**), N^2,$N^{2''}$-dihexyl-2'-(trimethylsilyl)-[1,1':3',1''-terphenyl]-2,2''-diamine (**12b**) and 2,2'-(2-(trimethylsilyl)-1,3-phenylene)bis(1-aminonaphthalen-2-yl) (**12c**), respectively, in yields of 87%, 82% and 65%. In the final cyclisation step, compounds **12a-c** were treated with BCl_3 and excess triethylamine at 180 °C to furnish the targeted NBN-edged PAHs **5a-b** and **6** via electrophilic borylation, which was directed by the central TMS group. The crude products were stable enough for purification by column chromatography on silica gel and recrystallization from $CHCl_3$/MeOH to furnish **5a-b** as colorless crystalline solids (yield of 90% and 87%). Recrystallization from THF/MeOH afforded π-extended derivative **6** as a light green powder (yield of 80%).

The stability of the NBN-DBPs allows further modifications of the skeleton that extend the π-conjugation and tune the optoelectronic properties of these heteroacenes. Thus, compound **5b** was successfully brominated with two equivalents of N-bromosuccinimide (NBS) to furnish 5,12-dibromo-8,9-dihexyl-8*H*,9*H*-8,9-diaza-8*a*-borabenzo[*fg*]tetracene (**13**) as a white solid in 87% yield, allowing for further functionalization through palladium-catalyzed cross-coupling reactions. For instance, Suzuki and Stille coupling reactions were performed with **13** to produce π-extended compounds substituted with phenyl and 2-thienyl moieties (**7a** (77%) and **7b** (85%), respectively) as colorless solids.

Inspired by the efficient cyclisation protocol, we aimed to synthesize an NBN-DBHZ **8** containing two 1,9-diaza-9*a*-boraphenalene motifs. Due to the decreasing solubility of these larger conjugated systems, we explored the synthesis of NBN-DBHZ **8** from a *N*-alkyl substituted quinquephenyl precursor (N^2,$N^{2''}$,$N^{2''''}$,$N^{5''}$-tetrahexyl-[1,1':3',1'':4'',1''':3''',1'''':quinquephenyl]-2,2'',2'''',5''-tetraamine, **17**). Compound 1,3-dibromobenzene (**9**) was reacted with 0.5 equivalent of boronic acid ester **3b** to furnish the mono-functionalized coupling product 3'-bromo-*N*-hexyl-[1,1'-biphenyl]-2-amine (**14**). This compound was then converted into the corresponding boronic acid ester, *N*-hexyl-3'-(4,4,5,5-tetramethyl-1,3,2-dioxaborolan-2-yl)-[1,1'-biphenyl]-2-amine (**15**) while using $Pd(dppf)Cl_2$ as a catalyst. The crude product was purified by flash column chromatography and used immediately for the next palladium-catalyzed reaction. Excess **15** was reacted with 2,5-dibromo-N^1,N^4-dihexylbenzene-1,4-diamine (**16**) to obtain **17** as a yellow oil in 73% yield. Finally, product **17** was treated with BCl_3 and triethylamine at 180 °C to afford pure NBN-DBHZ **8** as yellow crystalline solid (35% yield) after purification by column chromatography on silica gel and recrystallization from $CHCl_3$/MeOH.

Scheme 2. Synthesis of NBN-dibenzoheptazethrene (NBN-DBHZ).

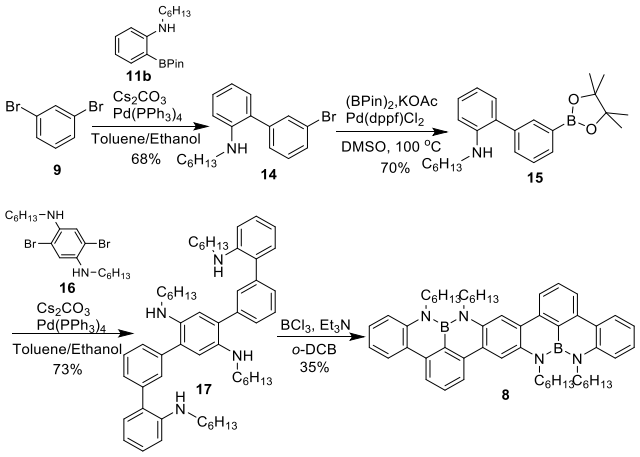

The intermediates and targeted compounds of NBN-DBPs and NBN-DBHZ were analysed by ^{1}H, ^{13}C and ^{11}B NMR spectroscopy, as well as HRMS. Notably, the broad peak of the amino hydrogen located at around 3.7 ppm in the ^{1}H NMR spectrum ($CDCl_3$) of intermediates **12a** disappeared after cyclisation to target molecule **5a**. For NBN-DBP **5a**, pronounced chemical shifts of protons at the nitrogen sites appeared at about 6.3 ppm, suggesting the aromatic character of BN-fused rings.[19] For the ^{1}H NMR spectrum ($CDCl_3$) of NBN-DBHZ **8**, there are two groups of triplet resonance peaks at 4.2 and 4.1 ppm, respectively, which are typically from the methylene protons neighbouring to the nitrogen, demonstrating the distinction of BN-fused rings in the higher homologue skeleton. In ^{11}B NMR, all the NBN-edged PAHs show one broad resonance around 26.7~30.6 ppm, which appears at significantly higher field compared to the reported heteroacenes with only BN-embedded structures (35~40 ppm).[20] These NBN-edged PAHs are stable toward ambient oxygen and moisture as solids. They also exhibit good thermal stability with a weight loss of 5% in the range of 250~350 °C based on thermal gravimetric analyses (Figure S1, Supporting Information).

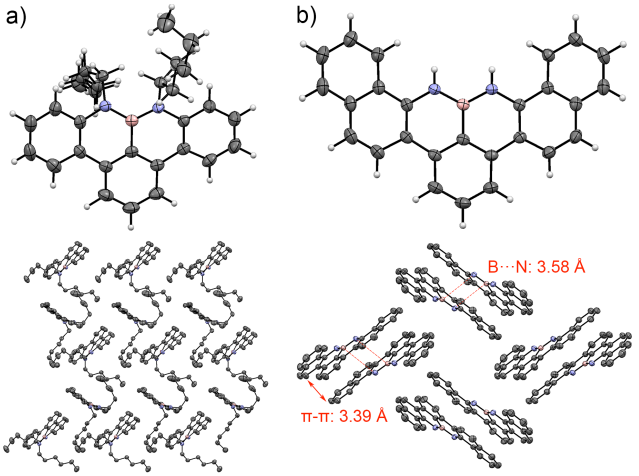

Figure 2. Crystal structures and packing diagrams for **5b** (a) and **6** (b).

X-ray Crystallographic Analysis. Single crystals of compounds **5b** and **7a**, which were suitable for X-ray structure analysis, were obtained by the slow evaporation of the chloroform solution. For compound **6** with poorer solubility, the suitable crystals were grown by the slow evaporation of its THF solution. All the crystal structures unambiguously reveal the structure of the defined N-B-N zigzag-edged periphery. Compound **5b** shows two types of slightly twisted conformations in one unit cell; the largest dihedral angle of 17.6° is probably due to the steric repulsion between the two alkyl chains (Figure 2a). Compound **5b** forms slipped stacks in a herringbone fashion through the many C–H···π interactions formed by the long alkyl chains, but no apparent π–π stacking interactions are observed. The B–N bond lengths in **5b** range from 1.42–1.44 Å, which are shorter than the analogous bond in typical BN-embedded PAHs (1.45 – 1.47 Å); these data indicate the presence of localized BN double bond character.[21] Compound **6** exhibits C_{2v}-symmetry with an essentially planar backbone; the largest dihedral angle among the fused rings is 2.9°. The two B–N bond lengths for **6** are approximately equivalent to each other at 1.42 Å. The packing diagram of compound **6** reveals a dimeric herringbone motif with an intermolecular BN dipole-dipole interactions (3.58 Å) which is below the sum of van der Waals radii (3.60 Å) (Figure 2b).[22] For compound **7a**, the central core shows a slightly twisted conformation with the largest dihedral angles of 14.4° similar to the structural characters of compound **5b** (Figure S2, SI).

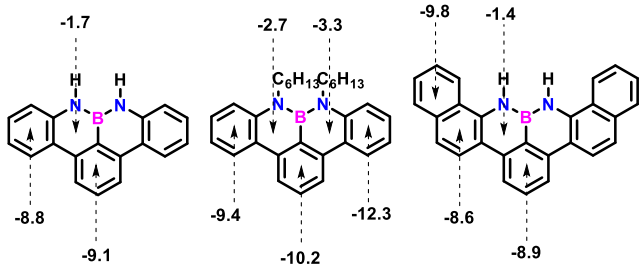

Figure 3. NICS(1) values (in ppm) of compounds **5a**, **5b** and **6** calculated at the GIAO-B3LYP/6-311+G(2d,p) level. The geometric data of **5b** and **6** were obtained from crystal structure, and the structure of **5a** is modified from **6**.

NICS Calculations. To understand how the NBN substitution influences the aromaticity of the dibenzophenalenes, we performed nucleus-independent chemical shift (NICS) calculations at the B3LYP/6-311+G(2d,p) level. As illustrated in Figure 3, the symmetrical NBN-DBP **5a** has a weakly aromatic phenalene core with a small negative NICS(1) value of -1.7 ppm for both BN rings and moderately aromatic features for the fused benzene rings. Similarly, the NICS(1) values for compound **6** are axisymmetric at -1.4 ppm for the BN rings. The peripheral benzene ring has a relatively negative NICS(1) value of -9.8 ppm, revealing more aromaticity than the rings (-8.6 and -8.9 ppm) adjacent to the BN core. Nevertheless, compound **5b** has different NICS(1) values, which may be caused by the steric repulsion between the alkyl chains according to the structural analysis.[23] Notably, the neighboring BN rings in **5b** have a stronger aromaticity (-2.7 and -3.3 ppm, respectively) than those of **5a**, which could be explained by the strengthened electron donating ability of the alkyl chains derived from the polarity of B-N bonds. The NICS(1) calculation results for the other NBN-edged PAHs are shown in Figure S3.

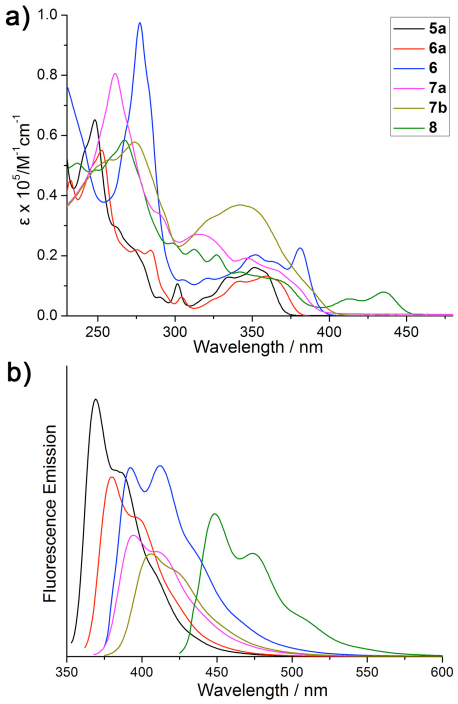

Figure 4. UV–vis absorption spectra (a) and emission spectra (b) of NBN-DBPs **5a**-**6**, arylated NBN-DBPs **7a**-**7b** and laterally extended NBN-DBHZ **8** at concentrations of 10^{-5} M in CH_2Cl_2.

Absorption and Emission Spectra. The UV-vis absorption spectra of the as-prepared NBN-edged PAHs are presented in Figure 4a. For NBN-DBPs **5a**-**5b**, two main absorption features are recorded in the wavelength regions of 250 – 300 nm and 300 – 400 nm along with the absorption maximum for the latter at λ = 351 nm and 359 nm (lg ε = 4.21 and 4.12), respectively, which are the wavelengths assigned to the π–π* transitions. The intensity of the peaks in the high-energy regions and the red shift (30 nm) of the absorption

maximum at λ = 381 nm (lg ε = 4.35) for **6** exceeded those of **5a**, these enhancements originate from the extended aromatic skeleton with the additional terminally fused benzene rings.[24] Compounds **7a** and **7b** both exhibit a red shifted absorption onset and stronger absorption intensity at approximately 300 – 400 nm when compared to **5b**. These results are attributed to the extended π-conjugation for **7a-b**, while the absorption maxima are blue shifted to 342 nm and 346 nm (lg ε = 4.28 and 4.57), respectively. For NBN-DBHZ **8**, the absorption maxima is shifted further to 435 nm (lg ε = 3.90). This large bathochromic shift is consistent with the extended conjugation in the higher homologue (**8**) with its repeated structural motif. The fluorescence of these compounds were also investigated (Figure 4b). Distinct blue shifts were found in the emission maxima of the as-prepared NBN-edged PAHs in the following sequence: **5a** (369 nm) < **5b** (380 nm) < **6** (393 nm) < **7a** (394 nm) < **7b** (406 nm) < **8** (448 nm). Notably, NBN-DBHZ **8** exhibits split emission bands at longer wavelengths, and it has a much higher fluorescence quantum yield (Φ_{PL}) (0.83) than smaller homologs **5a-7b**.[25]

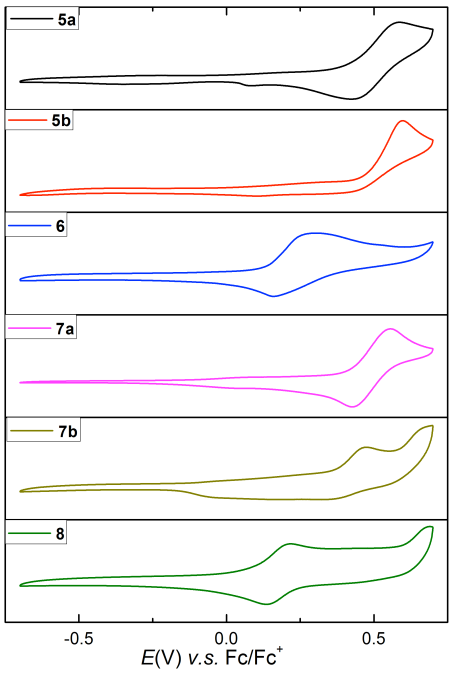

Figure 5. Cyclic voltammograms of NBN-DBPs **5a-7b** and NBN-DBHZ **8** measured in CH_2Cl_2 (0.1 mol/L n-Bu_4NPF_6) at a scan rate of 100 mV/s. The compounds were scanned for their first oxidation potential.

Electrochemical Properties. The electrochemical behavior of the NBN-DBPs (**5a-7b**) and NBN-DBHZ **8** were investigated by cyclic voltammetry (CV). The compounds were scanned for their first oxidation potential in CH_2Cl_2 as shown in Figure 5. Compounds **5a** showed a quasi-reversible wave at 0.51 V. The cyclic voltammetry of **5a** was also performed in acetonitrile. Interestingly, besides an irreversible redox wave at a higher potential, a new reversible redox peak appeared at a lower potential upon a multi-cycle scanning, suggesting the formation of possible oligomers or polymers (Figure 6c), and the follow-up experiments proved the σ-dimer structure (see below).[31] NBN-DBP **5b,** with alkyl substituents at nitrogen atoms, offered an irreversible peak at 0.60 V. A quasi-reversible peak at 0.25 V was observed for **6**, much lower than **5b**, due to the extended π-conjugated skeleton of the former one. Interestingly, **7a** terminated with phenyl substituents in the lateral sides, showed an one-electron reversible redox peak at 0.49 V, while **7b** gave an irreversible wave at 0.47 V, probably because of its thiophene terminal groups with electrochemical activity.[26] The first oxidation potential for **7a** or **7b** is remarkably lower than those of **5a** and **5b**, suggesting that the introduction of aromatic units in the N-*para* position of such kinds of NBN-DBPs enable extending π-conjugation. Among these molecules, the CV profile of NBN-DBHZ **8** exhibits one quasi-reversible oxidation wave at the lowest potential of 0.18 V with respect to its largest π-conjugated backbone. Obviously, the significant differences in the CV profiles of these compounds are highly associated with their intrinsic molecular structures, and even a tiny variation of these molecular structures would cause a significant change in their electrochemical behavior. Accordingly, the HOMO energy levels of the as-prepared NBN-edged PAHs were evaluated from the onsets of the first oxidation potential. The low-lying HOMO energy levels of these NBN-DBPs **5a-b** and **7a-7b** (-5.26~-5.36 eV) suggest that these compounds are promising candidates for air-stable p-type semiconductors.[27] Moreover, the LUMO energy level was calculated based on the HOMO values and the optical bandgaps (Table 1).

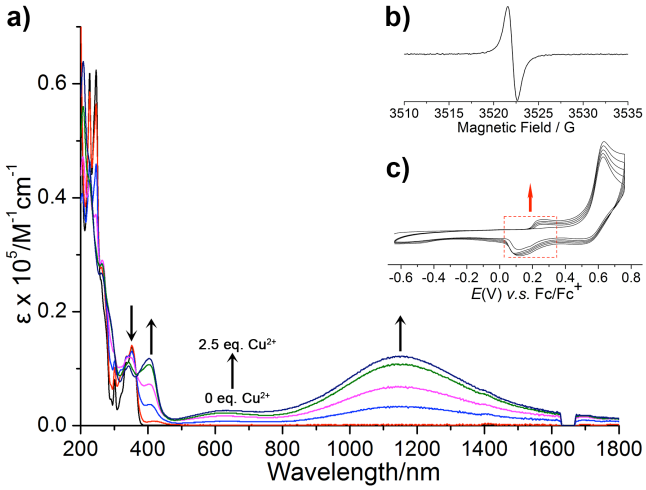

Figure 6. (a) UV–vis-NIR absorption spectra of **5a** titrated with $Cu(OTf)_2$ (0, 0.5, 1.0, 1.5, 2.0, 2.5 e.q.) at concentrations of 10^{-5} M in acetonitrile. (b) EPR spectrum of the reaction solution of $Cu(OTf)_2$ + **5a** at 10^{-3} M in acetonitrile. (c) Cyclic voltammograms of **5a** measured in acetonitrile (0.1 mol/L n-Bu_4NPF_6) at a scan rate of 100 mV/s.

Chemical oxidation of NBN-DBPs. Encouraged by the electrochemical behavior of NBN-DBPs, we firstly examined the chemical oxidation of **5a** as a typical example. Given its quasi-reversible redox process with the first oxidation potential of E^1_{ox}=0.59 V (vs Fc/Fc^+), an exergonic thermal electron transfer (ET) ($\Delta G_{ET} < 0$) to Cu^{2+} to form the radical cation can be predicted.[28] Indeed, titration of **5a** by $Cu(OTf)_2$ showed a large bathochromic shift, indicating the formation of radical cationic species based on the *in-situ* Vis-NIR absorption spectroscopy (Figure 6a).[29] With the progressive addition of $Cu(OTf)_2$, a set of new absorption peaks in the visible and NIR regions of **5a** gradually evolved at 404, 620,

and 1150 nm with a concomitant decrease of the π-π* transition bands at 336 and 352 nm. A well-defined isosbestic point

Table 1. Photochemical and electrochemical properties of the NBN-edged PAHs.

	UV-vis absorption			Fluorescence		Electrochemistry		DFT calculations	
	λ_{abs}[a] (nm)	log ε	E_g[b] (eV)	λ_{em} (nm)	Φ_{PL}[c]	HOMO[d] (eV)	LUMO[e] (eV)	IP[f] (eV)	EA[f] (eV)
5a	351	4.21	3.35	369	0.24	-5.31	-1.96	5.63	1.51
5b	359	4.12	3.26	380	0.21	-5.36	-2.10	5.70	1.28
6	381	4.35	3.15	393	0.26	-5.06	-1.91	5.42	1.59
7a	342	4.28	3.15	394	0.19	-5.32	-2.17	5.65	1.34
7b	346	4.57	3.08	406	0.09	-5.26	-2.16	5.61	1.42
8	435	3.90	2.74	448	0.83	-4.99	-2.25	5.32	1.56

[a]Absorption wavelength of the first absorption maximum. [b]Estimated from the UV-vis absorption edge. [c]Absolute value. [d]Calculated from the onset of the first oxidation wave using HOMO = $-E_{ox1}$ – 4.80 eV. [e]Estimated according to LUMO = HOMO + E_g. [f]The polarization and relaxation corrected ionization potential (IP) and electron affinity (EA) correspond to the HOMO and LUMO states, respectively (see SI for more details).

at 367 nm could be clearly identified. Moreover, upon addition of $Cu(OTf)_2$ in acetonitrile at 10^{-3} M, the electron paramagnetic resonance (EPR) spectrum revealed a strong signal at g = 2.0033 with a peak-to-peak width of 1 G (Figure 6b), without any hyperfine coupling observed. This result suggests many different coupling from a highly delocalized structure, over which the spin density of the unpaired electron is distributed.[30] Meanwhile, the extremely rapid and distinct change from colorless solution to deep green suspension could also be observed by naked eyes. To exclude the EPR-active interference of Cu, we also used the EPR-inactive oxidant $NOBF_4$ for the oxidation of compound **5a**, and under the same condition, we detected the similar but weaker EPR signal (Figure S4, SI).

Scheme 3. Plausible oxidation process of 5a.

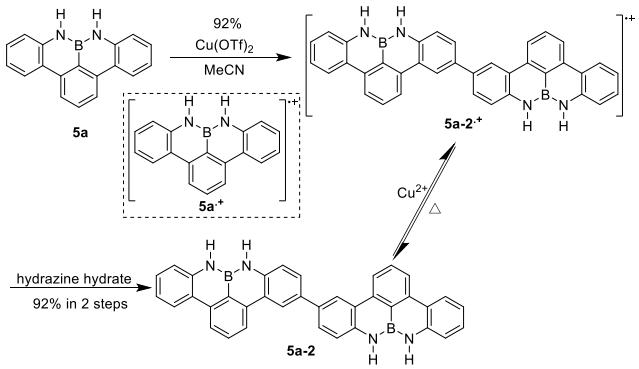

In order to gain further insight into these interesting results, reaction of **5a** with $Cu(OTf)_2$ in acetonitrile was carried out in preparative scale (Scheme 3). Treatment of **5a** with two equimolar $Cu(OTf)_2$ under nitrogen atmosphere gave a deep green suspension in the early stage of the reaction, which resembled the UV-vis-NIR and EPR studies of the initial *in-situ* investigation. Afterwards, two different workup methods have been employed. In the first one we added excess hydrazine hydrate to the resulting suspension, leading to a color change from deep green to milky white. After filtration, a new compound (donated as **5a-2**) with good purity was collected as white powder in a yield of 92%, which was first characterized by ^{1}H NMR spectra. In comparison with only one broad peak at 8.24 ppm with respect to nitrogen protons for **5a**, ^{1}H NMR spectra (DMSO-$_{d6}$) of **5a-2**, showed the two broad peaks at 8.30 and 8.34 ppm, respectively, assignable to the different nitrogen protons on the phenalene scaffold (Figure S5-6, SI). On the basis of 2D-NMR analyses (Page S35-49, SI), **5a-2** was unambiguously confirmed as N-*para* C-C coupling dimer,[32] also in accordance with the result by MALDI-TOF MS analyses. The other method is that the deep green suspension was directly filtered to afford dark green powder without the addition of any reductant. The resulting powder dissolved in DMSO-$_{d6}$ as green solution was NMR silent at room temperature, suggesting the existence of an unpaired electron, while after heating for several minutes in the air, the green solution was transformed to a colorless one, and showing a set of proton signals, consistent with that of the neutral dimer **5a-2** (Figure S7, SI). Combined with well-resolved MALDI-TOF MS, ESI^--MS spectra, as well as EPR spectra, the formation of the radical cation of **5a** dimer with OTf^- counter anion (denoted as **5a-2**$^{\bullet+}\cdot OTf^-$), can be confirmed (Page S50, S55, and Figure S8, SI). Therefore, **5a** undergoing oxidative dimerization via an open-shell intermediate is proposed as shown in Scheme 3. The conversion between the neutral dimer and dimer radical cation can be smoothly conducted by a simple redox treatment, as validated by cyclic voltammetry and UV-vis-NIR absorption spectroscopy (Figure S9-12, SI).

Similarly, N-alkyl NBN-DBP **5b** also could be nearly quantitatively converted to the dimer **5b-2** as white powder upon the oxidation treatment. The molecular structure of **5b-2** through N-*para* C-C linkage, similar to **5a-2**, was clearly confirmed by ^{1}H, ^{13}C NMR spectra and HR-

MALDI-TOF MS analyses. On the contrary, for compound **7a**, the phenyl substituents at the N-*para* position should block the formation of similar dimers, which indeed is confirmed upon chemical oxidation (Page S51-52, SI). Such result is highly consistent with its reversible electrochemical behavior aforementioned, and clearly demonstrates the highly regioselective activity of such kinds of NBN-edged PAHs.

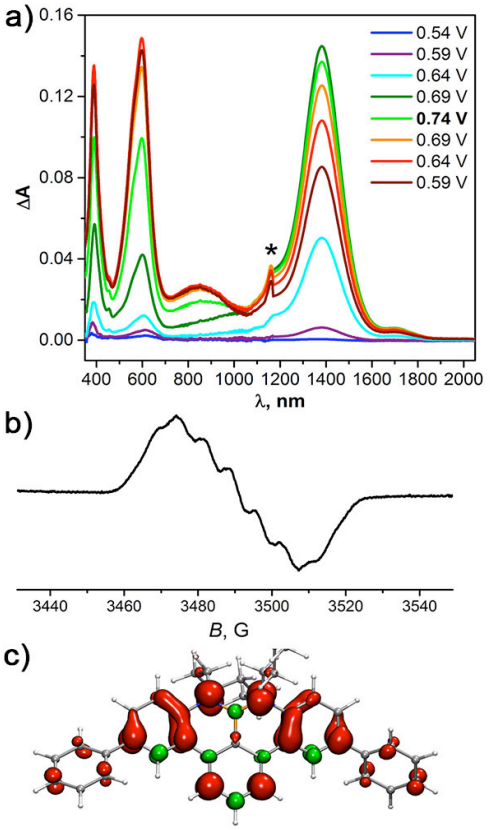

Figure 7. (a) Selected Vis-NIR absorption spectra measured in situ during cyclic voltammetry of **7a** at its first oxidation peak, vertex potential is 0.74 V *v.s.* Fc/Fc^+ (The asterisk at 1180 nm denotes an artefact of the spectrometer due to the change of detector channels). (b) EPR spectrum of $\mathbf{7a}^{\bullet+}$ cation radical measured in situ during electrochemical oxidation of **7a** at the potential of 0.59 V. (c) DFT-computed spin-density distribution in the $\mathbf{7a}^{\bullet+}$ (red "+", green "–", alkyl chains are abridged for clarity). These calculations were performed using Orca package at the B3LYP level using def2-TZVP basis set for C and specially tailored EPR-III basis set for H, N, and B.

***In-situ* spectroelectrochemistry for NBN-DBPs.** To understand the formation process of radical cation $\mathbf{5a\text{-}2}^{\bullet+}$ in more detail, we further performed *in-situ* spectroelectrochemistry (SEC) for compound **5a** in acetonitrile. At a low scan rate of 2.5 mV/s. electrochemical oxidation was followed by a chemical reaction, which formed a new compound with an oxidation potential near 0.25 V (Figure S13, SI). *In-situ* EPR/Vis-NIR spectroelectrochemical studies showed that oxidation of **5a** in acetonitrile caused appearance of absorption band at 1100 nm accompanied by a relatively narrow EPR signal at g = 2.0027 with a linewidth of 0.7 G. These spectroscopic features are similar to those observed for the solution of the precipitate formed during chemical oxidation of **5a** by Cu^{2+} as discussed in the chemical oxidation section. In addition, the oxidation potential of the dimer **5a-2** coincides with the oxidation potential of the follow-up products of the electrochemical oxidation of **5a** (Figure S14, SI). These results thus enable us to conclude that precipitate observed in the chemical oxidation of **5a** is a cation-radical $\mathbf{5a\text{-}2}^{\bullet+}$ (see detail structure in Figure S15, SI). The SEC studies also showed that absorption intensity at 1100 nm increased almost twice at the second voltammetric cycle, and the formation of the film was observed on the electrode after the measurements. Presumably, **5a** not only dimerized upon electrochemical oxidation, but underwent a further electropolymerization.

For comparison, we also peformed the *in-situ* SEC studies for NBN-DBP **7a**. Obviously, phenyl substitutions at N-*para* positions (which are dimerization sites in **5a**) prevent dimerization/polymerization of **7a**. *In-situ* EPR/Vis-NIR measurements during electrochemical oxidation revealed absorption bands of the $\mathbf{7a}^{\bullet+}$ radical cation at 598 and 1380 nm and a broad EPR signal at g = 2.0026 with the sign of hyperfine structure (Figure 7a-b and Figure S16, SI). DFT-computations show that the spin density in $\mathbf{7a}^{\bullet+}$ is delocalized over the whole π-system (Figure 7c), which results in relatively large hyperfine constants for many nuclei. In particular, the largest hyperfine coupling constants (hfcc) values are predicted for B (–13.5 MHz), one of the protons in the CH_2 groups next to the atoms of nitrogen (16.0 and 18.0 MHz), N (2 × 9.9 MHz), and two protons at 4,6-boraphenalene positions (2 × –8.3 MHz). Hyperfine constants for other protons are less than 3 MHz (Figure S17, SI). A combination of many magnetic nuclei with a broad distribution of hfcc values gives a broad EPR signal with a rich hyperfine structure, which cannot be fully resolved.

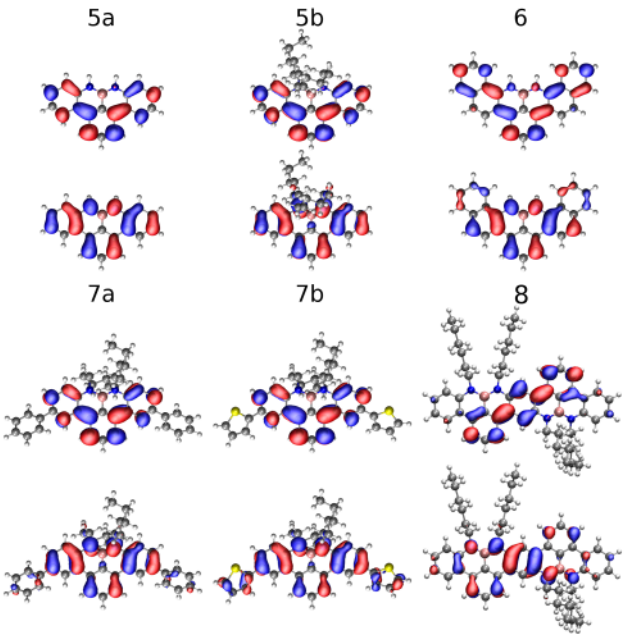

Figure 8. LUMO (upper panels) and HOMO (lower panels) of NBN-edged PAHs **5a**-**8** obtained from DFT calculations.

Spectroscopic Calculations. We further performed density functional theory (DFT) calculations using the Gaussian09 software package[33] at the M06-2X/cc-pVTZ level[34] to characterize the electronic structure of all NBN-DBPs and their absorption spectra, as shown in Table 1 and Figure 8-9 (see SI for more details). For all the molecules except compound **6,** the HOMO (LUMO) frontier orbital is separated by more than 0.4 eV from lower (higher) energy levels. For **6**, the LUMO and the LUMO+1 are close with an energy separation of 0.14 eV. The frontier orbitals of compounds **5a-b**, **6**, and **7a-b** have similar shapes and exhibit a nodal structure that keeps the boron atom clear of weight (Figure 8). The HOMO is partially localized at the nitrogen atoms, while the LUMOs have no weight at that point. For molecule **6** the frontier molecular orbitals are even more strongly delocalized over the entire molecule, leading to a reduced ionization potential (IP), a smaller energy gap, and a further red shift in the absorption spectrum (Figure 9), remaining consistent with the experimental CV and UV-vis-NIR results. The dominant absorption peak doublet above 350 nm is caused by the energetic proximity of the LUMO and LUMO+1 levels, which are both involved in the electronic transitions. Frontier MOs with greater π-delocalization are observed in NBN-DBHZ **8**, leading to a further decrease in the HOMO-LUMO gap and a red shift in the absorption, in agreement with the UV-vis-NIR results. Functionalizing **5b** to obtain **7a** and **7b** increases the absorption intensity, while the IP, electron affinity (EA) values and absorption onsets are almost unchanged, corroborating our experimental observations. In addition, we found that the simulated absorption spectra of **5a-2** in various oxidation forms also showed strong absorption in the NIR region similar to the experimental findings, consistent with the reaction of the **5a** monomer to the **5a-2** dimer structure (Figure S18-20, see detailed discussion in SI).

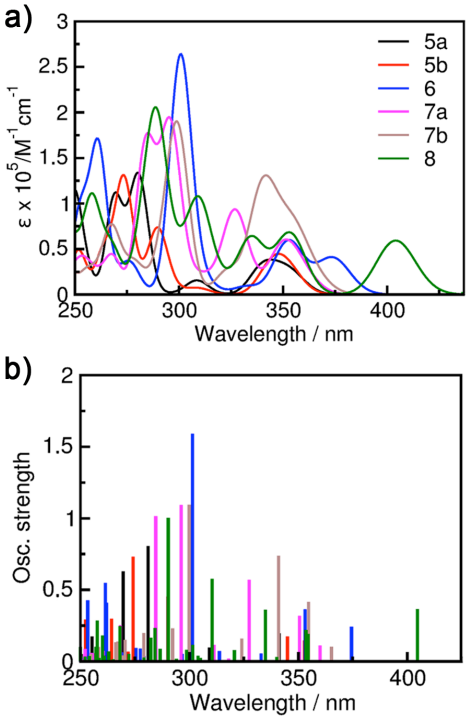

Figure 9. (a) Simulated absorption spectra with Gaussian-type linewidth broadening (σ=0.1 eV). (b) Simulated excitation energies versus corresponding oscillator strengths. To reduce a systematic offset relative to the experimental data, a polarization shift to account for solvation effects has been applied (see SI).

CONCLUSIONS

In summary, a synthetic route toward unprecedented heteroatom-doped PAHs featuring a nitrogen-boron-nitrogen-type zigzag-edged periphery was introduced based on a 1,9-diaza-9*a*-boraphenalene core structure. Alternating nitrogen and boron atoms imparts high chemical stability to these zigzag-edged PAHs; this motif even allows for post-synthetic modifications. The possibilities for lateral extension were demonstrated by the synthesis of the higher homologue **8,** suggesting that NBN-doped zigzag-edged graphene nanoribbons could be synthesized via this route.[35] Upon chemical oxidation, as an example, NBN-DBP **5a** was nearly quantitatively converted to a N-*para* C-C linked dimer through an open-shell intermediate, revealing the highly regioselective activation of NBN-DBPs at molecular peripheries. By additional phenyl substituentions in **7a**, oligomerization can be prevented and the clean single-electron oxidation of NBN into the isoelectronic allyl radical can be performed by means of *in-situ* spectroelectrochemistry, generating radical cation **7a**$^{\cdot+}$ as isoelectronic to the unprecedented full-carbon dibenzophenalenyl radical. This work provides a new class of PAH molecules with tunable properties while promoting our strategy to obtain tailor-made, complex architectures, such as conjugated polymers,[36] dendrimers,[37] organic framework materials,[38] and graphene nanoribbons with stable NBN-doped zigzag-edged peripheries.

ASSOCIATED CONTENT

Supporting Information

The Supporting Information is available free of charge on the ACS Publications website at DOI: 10.1021/jacs.XXXXXX.

Experimental details, TGA spectra, single-crystal X-ray diffraction data, *in-situ* SEC results, computational details, NMR spectra and HRMS spectra. (PDF)

Crystallographic information files for compounds **5b**, **6**, **7a** and **13**. (CIF)

AUTHOR INFORMATION

Corresponding Author

* fan-zhang@sjtu.edu.cn

* xinliang.feng@tu-dresden.de

Notes

The authors declare no competing financial interest.

ACKNOWLEDGMENT

We are grateful for the financial supported from the National Basic Research Program of China (973 Program: 2013CBA01602, 2012CB933404), the Natural Science Foundation of China (21574080), and the Shanghai Committee of Science and Technology (15JC1490500).

REFERENCES

(1) (a) Morita, Y.; Suzuki, S.; Sato, K.; Takui, T. *Nat. Chem.* **2011**, *3*, 197. (b) Li, Y.; Heng, W.-K.; Lee, B. S.; Aratani, N.; Zafra, J. L.; Bao, N.; Lee, R.; Sung, Y. M.; Sun, Z.; Huang, K.-W.; Webster, R. D.; López Navarrete, J. T.; Kim, D.; Osuka, A.; Casado, J.; Ding, J.; Wu, J. *J. Am. Chem. Soc.* **2012**, *134*, 14913. (c) Li, Y.; Huang, K.-W.; Sun, Z.; Webster, R. D.; Zeng, Z.; Zeng, W.; Chi, C.; Furukawa, K.; Wu, J. *Chem. Sci.* **2014**, *5*, 1908. (d) Ruffieux, P.; Wang, S.; Yang, B.; Sánchez-Sánchez, C.; Liu, J.; Dienel, T.; Talirz, L.; Shinde, P.; Pignedoli, C. A.; Passerone, D.; Dumslaff, T.; Feng, X.; Müllen, K.; Fasel, R. *Nature* **2016,** *531*, 489.

(2) Goto, K.; Kubo, T.; Yamamoto, K.; Nakasuji, K.; Sato, K.; Shiomi, D.; Takui, T.; Kubota, M.; Kobayashi, T.; Yakusi, K. *J. Am. Chem. Soc.* **1999**, *121*, 1619.

(3) (a) Cofino, W. P.; van Dam, S. M.; Kamminga, D. A.; Hoornweg, G. P.; Gooijer, C.; MacLean, C.; Velthorst, N. H. *Mol. Phys.* **1984,** *51*, 537. (b) O'Connor, G. D.; Troy, T. P.; Roberts, D. A.; Chalyavi, N.; Fückel, B.; Crossley, M. J.; Nauta, K.; Stanton, J. F.; Schmidt, T. W. *J. Am. Chem. Soc.* **2011**, *133*, 14554.

(4) O'Brien, S.; Smith, D. C. C. *J. Chem. Soc.* **1963**, 2907.

(5) Rotermund, G. W.; Köster, R. Justus Liebigs Annalen der Chemie **1965**, *686*, 153.

(6) Clar, E.; Fell, G. S.; Richmond, M. H. *Tetrahedron* **1960**, *9*, 96.

(7) (a) Berger, R.; Giannakopoulos, A.; Ravat, P.; Wagner, M.; Beljonne, D.; Feng, X.; Müllen, K. *Angew. Chem., Int. Ed.* **2014**, 53, 10520. (b) Berger, R.; Wagner, M.; Feng, X.; Müllen, K. *Chem. Sci.* **2015**, *6*, 436.

(8) (a) Liu, Z.; Marder, T. B. *Angew. Chem., Int. Ed.* **2008**, *47*, 242. (b) Bosdet, M. J. D.; Piers, W. E. *Can. J. Chem.* **2009**, 87, 8. (c) Campbell, P. G.; Marwitz, A. J. V.; Liu, S.-Y. *Angew. Chem., Int. Ed.* **2012**, *51*, 6074. (d) Wang, X. -Y.; Wang, J. Y.; Pei, J. *Chem.- Eur. J.* **2015,** *21*, 3528.

(9) (a) Aramaki, Y.; Orniya, H.; Yamashita, M.; Nakabayashi, K.; Ohkoshi, S.-i.; Nozaki, K. *J. Am. Chem. Soc.* **2012,** *134*, 19989. (b) Suzuki, S.; Yoshida, K.; Kozaki, M.; Okada, K. *Angew. Chem., Int. Ed.* **2013,** 52, 2499. (c) Rosenthal, A. J.; Devillard, M.; Miqueu, K.; Bouhadir, G.; Bourissou, D. *Angew. Chem., Int. Ed.* **2015,** *54*, 9198.

(10) (a) Agou, T.; Kobayashi, J.; Kawashima, T. *Org. Lett.* **2006,** *8*, 2241. (b) Li, G.; Wu, Y.; Gao, J.; Wang, C.; Li, J.; Zhang, H.; Zhao, Y.; Zhao, Y.; Zhang, Q. *J. Am. Chem. Soc.* **2012**, *134*, 20298. (c) Dou, C. D.; Saito, S.; Matsuo, K.; Hisaki, I.; Yamaguchi, S. *Angew. Chem., Int. Ed.* **2012,** *51*, 12206. (d) Neue, B.; Araneda, J. F.; Piers, W. E.; Parvez, M. *Angew. Chem., Int. Ed.* **2013,** 52, 9966. (e) Tang, R.; Zhang, F.; Fu, Y.; Xu, Q.; Wang, X.; Zhuang, X.; Wu, D.; Giannakopoulos, A.; Beljonne, D.; Feng, X. *Org. Lett.* **2014**, *16*, 4726.

(11) (a) Sumida, Y.; Harada, R.; Kato-Sumida, T.; Johmoto, K.; Uekusa, H.; Hosoya, T. *Org. Lett.* **2014**, *16*, 6240. (b) Katayama, T.; Nakatsuka, S.; Hirai, H.; Yasuda, N.; Kumar, J.; Kawai, T.; Hatakeyama, T. *J. Am. Chem. Soc.* **2016**, *138*, 5210.

(12) Wang, X.-Y.; Narita, A.; Zhang, W.; Feng, X.; Müllen, K. *J. Am. Chem. Soc.* **2016**, *138*, 9021.

(13) Narita, A.; Wang, X. Y.; Feng, X.; Müllen, K. *Chem. Soc.* Rev. **2015**, *44*, 6616.

(14) (a) Riehm, T.; De Paoli, G.; Wadepohl, H.; De Cola, L.; Gade, L. H. *Chem. Commun.* **2008**, *42*, 5348. (b) Nishida, J.-i.; Fujita, T.; Fujisaki, Y.; Tokito, S.; Yamashita, Y. *J. Mater. Chem.***2011**, *21*, 16442. (c) Abbey, E. R.; Liu, S.-Y. *Org. Biomol. Chem.* **2013**, *11*, 2060.

(15) Lorenz, T.; Lik, A.; Plamper, F. A.; Helten, H. *Angew. Chem., Int. Ed.* **2016**, 55, 7236.

(16) During the preparation of this manuscript, Hatakeyama et al. reported the synthesis of N-methylic NBN-DBP via demethylative direct borylation: Numano, M.; Nagami, N.; Nakatsuka, S.; Katayama, T.; Nakajima, K.; Tatsumi, S.; Yasuda, N.; Hatakeyama, T. *Chem.- Eur. J.* **2016**, *22*, 11574.

(15) Clar, E.; Fell, G. S.; Richmond, M. H. *Tetrahedron* **1960**, *9*, 96.

(17) Wang, X.; Zhang, F.; Gao, J.; Fu, Y.; Zhao, W.; Tang, R.; Zhang, W.; Zhuang, X.; Feng, X. *J. Org. Chem.* **2015**, *80*, 10127..

(18) Mongin, F.; Marzi, E.; Schlosser, M. *Eur. J. Org. Chem.* **2001**, *2001*, 2771.

(19) (a) Wang, X.; Zhang, F.; Liu, J.; Tang, R.; Fu, Y.; Wu, D.; Xu, Q.; Zhuang, X.; He, G.; Feng, X., *Org. Lett.* **2013**, *15*, 5714. (b) Wang, X.-Y.; Zhuang, F.-D.; Wang, X.-C.; Cao, X.-Y.; Wang, J.-Y.; Pei, J. *Chem. Commun.* **2015**, *51*, 4368.

(20) (a) Wang, X. -Y.; Lin, H. R.; Lei, T.; Yang, D. C.; Zhuang, F. D.; Wang, J. Y.; Yuan, S. C.; Pei, J. *Angew. Chem., Int. Ed.* **2013,** 52, 3117. (b) Wang, X.-Y.; Zhuang, F.-D.; Wang, R.-B.; Wang, X.-C.; Cao, X.-Y.; Wang, J.-Y.; Pei, J. *J. Am. Chem. Soc.* **2014**, *136*, 3764. (c) Ishibashi, J. S.; Marshall, J. L.; Maziere, A.; Lovinger, G. J.; Li, B.; Zakharov, L. N.; Dargelos, A.; Graciaa, A.; Chrostowska, A.; Liu, S.-Y. *J. Am. Chem. Soc.* **2014**, *136*, 15414.

(21) (a) Lepeltier, M.; Lukoyanova, O.; Jacobson, A.; Jeeva, S.; Perepichka, D. F. *Chem. Commun.* **2010**, *46*, 7007. (b) Hatakeyama, T.; Hashimoto, S.; Seki, S.; Nakamura, M. *J. Am. Chem. Soc.* **2011**, 133, 18614. (c) Müller, M.; Maichle-Mossmer, C.; Bettinger, H. F. *Angew. Chem., Int. Ed.* **2014**, 53, 9380.

(22) Jaska, C. A.; Emslie, D. J. H.; Bosdet, M. J. D.; Piers, W. E.; Sorensen, T. S.; Parvez, M. *J. Am. Chem. Soc.* **2006**, *128*, 10885.

(23) Schaffroth, M.; Gershoni-Poranne, R.; Stanger, A.; Bunz, U. H. F. *J. Org. Chem.* **2014**, *79*, 11644.

(24) (a) Niimi, K.; Shinamura, S.; Osaka, I.; Miyazaki, E.; Takimiya, K. *J. Am. Chem. Soc.* **2011,** *133*, 8732. (b) Mori, T.; Nishimura, T.; Yamamoto, T.; Doi, I.; Miyazaki, E.; Osaka, I.; Takimiya, K. *J. Am. Chem. Soc.* **2013**, *135*, 13900.

(25) Wetzel, C.; Brier, E.; Vogt, A.; Mishra, A.; Mena-Osteritz, E.; Bäuerle, P. *Angew. Chem., Int. Ed.* **2015**, *54*, 12334.

(26) (a) Waltman, R. J.; Diaz, A. F.; Bargon, J. *J. Phys. Chem.* **1984,** *88*, 4343. (b) Roncali, J. *Chem. Rev.* **1992,** *92*, 711. (c) Lukoyanova, O.; Lepeltier, M.; Laferrière, M.; Perepichka, D. F. *Macromolecules* **2011,** *44*, 4729.

(27) (a) Gao, J. H.; Li, R. J.; Li, L. Q.; Meng, Q.; Jiang, H.; Li, H. X.; Hu, W. P. *Adv. Mater.* **2007**, *19*, 3008. (b) Wang, C.; Dong, H.; Hu, W.; Liu, Y.; Zhu, D. *Chem. Rev.* **2011,** *112*, 2208.

(28) The redox potential of Cu2+/Cu+ couple was estimated to be +0.65 V vs Fc+/Fc. (a) Cox, B. G.; Jedral, W.; Palou, *J. Chem. Soc., Dalton Trans.* **1988**, *3*, 733. (b) Connelly, N. G.; Geiger, W. E. *Chem. Rev.* **1996,** *96*, 877.

(29) (a) Ajayakumar, M.; Asthana, D.; Mukhopadhyay, P. *Org. Lett.* **2012,** *14*, 4822. (b) Wu, X.; Guo, Z.; Wu, Y.; Zhu, S.; James, T. D.; Zhu, W. *ACS Appl. Mater. Inter.* **2013,** *5*, 12215. (c) Jung, J. Y.; Kang, M.; Chun, J.; Lee, J.; Kim, J.; Kim, J.; Kim, Y.; Kim, S.-J.; Lee, C.; Yoon, J. *Chem. Commun.* **2013,** *49*, 176.

(30) Ji, L.; Edkins, R. M.; Lorbach, A.; Krummenacher, I.; Brückner, C.; Eichhorn, A.; Braunschweig, H.; Engels, B.; Low, P. J.; Marder, T. B. *J. Am. Chem. Soc.* **2015,** *137*, 6750.

(31) (a) Smie, A.; Heinze, J. *Angew. Chem., Int. Ed.* **1997,** *36*, 363. (b) Heinze, J.; Willmann, C.; Bäuerle, P. *Angew. Chem., Int. Ed.* **2001,** *40*, 2861. (c) Chen, X.; Wang, X.; Zhou, Z.; Li, Y.; Sui, Y.; Ma, J.; Wang, X.; Power, P. P. *Angew. Chem., Int. Ed.* **2013,** *52*, 589.

(32) Some N-*para* σ-dimer examples: (a) Kamada, K.; Fuku-en, S.-i.; Minamide, S.; Ohta, K.; Kishi, R.; Nakano, M.; Matsuzaki, H.; Okamoto, H.; Higashikawa, H.; Inoue, K. *J. Am. Chem. Soc.* **2012,** *135*, 232. (b) Zheng, X.; Wang, X.; Qiu, Y.; Li, Y.; Zhou, C.; Sui, Y.; Li, Y.; Ma, J.; Wang, X. *J. Am. Chem. Soc.* **2013,** *135*, 14912. Biphenalenylidene examples: (c) Uchida, K.; Ito, S.; Nakano, M.; Abe, M.; Kubo, T. *J. Am. Chem. Soc.* **2016**, *138*, 2399. (d) Uchida, K.; Mou, Z.; Kertesz, M.; Kubo, T. *J. Am. Chem. Soc.* **2016**, *138*, 4665.

(33) Gaussian 09, Revision D.01, Frisch, M. J.; Trucks, G. W.; Schlegel, H. B.; Scuseria, G. E.; Robb, M. A.; Cheeseman, J. R.; Scalmani, G.; Barone, V.; Mennucci, B.; Petersson, G. A.; Nakatsuji, H.; Caricato, M.; Li, X.; Hratchian, H. P.; Izmaylov, A. F.; Bloino, J.; Zheng, G.; Sonnenberg, J. L.; Hada, M.; Ehara, M.; Toyota, K.; Fukuda, R.; Hasegawa, J.; Ishida, M.; Nakajima, T.; Honda, Y.; Kitao, O.; Nakai, H.; Vreven, T.; Montgomery, Jr., J. A.; Peralta, J. E.; Ogliaro, F.; Bearpark, M.; Heyd, J. J.; Brothers, E.; Kudin, K. N.; Staroverov, V. N.; Kobayashi, R.; Normand, J.; Raghavachari, K.; Rendell, A.; Burant, J. C.; Iyengar, S. S.; Tomasi, J.; Cossi, M.;Rega, N.; Millam, N. J.; Klene, M.; Knox, J. E.; Cross, J. B.; Bakken, V.; Adamo, C.; Jaramillo, J.; Gomperts, R.; Stratmann, R. E.; Yazyev, O.; Austin, A. J.; Cammi, R.; Pomelli, C.; Ochterski, J. W.; Martin, R. L.; Morokuma, K.; Zakrzewski, V. G.; Voth, G. A.; Salvador, P.; Dannenberg, J. J.; Dapprich, S.; Daniels, A. D.; Farkas, Ö.; Foresman, J. B.; Ortiz, J. V.; Cioslowski, J.; Fox, D. J. Gaussian, Inc., Wallingford CT, **2009**.

(34) (a) Zhao, Y.; Truhlar, D. G. *Theor. Chem. Acc.* **2008**, *120*, 215. (b) Dunning, T. H. *J. Chem. Phys.* **1989**, *90*, 1007. (c) Kendall, R. A.; Dunning, T. H.; Harrison, R. J. *J. Chem. Phys.* **1992**, *96*, 6796.

(35) (a) Narita, A.; Feng, X.; Hernandez, Y.; Jensen, S. A.; Bonn, M.; Yang, H.; Verzhbitskiy, I. A.; Casiraghi, C.; Hansen, M. R.; Koch, A. H. *Nat. Chem.* **2014**, *6*, 126. (b) Bunz, U. H. F. *Accounts Chem. Res.* **2015**, *48*, 1676.

(36) (a) Jäkle, F. *Chem. Rev.* **2010**, *110*, 3985. (b) Lei, T.; Wang, J.-Y.; Pei, J. *Accounts Chem. Res.* **2014**, *47*, 1117. (c) Baggett, A. W.; Guo, F.; Li, B.; Liu, S.-Y.; Jäkle, F. *Angew. Chem., Int. Ed.* **2015**, *54*, 11191.

(37) (a)Vögtle, F.; Gestermann, S.; Hesse, R.; Schwierz, H.; Windisch, B. *Prog. Polym. Sci.* **2000,** *25*, 987. (b) Hammer, B. A. G.; Moritz, R.; Stangenberg, R.; Baumgarten, M.; Müllen, K. *Chem. Soc. Rev.* **2015**, *44*, 4072.

(38) (a) Feng, X.; Ding, X.; Jiang, D. *Chem. Soc. Rev.* **2012**, *41*, 6010. (b) Kawasumi, K.; Zhang, Q.; Segawa, Y.; Scott, L. T.; Itami, K. *Nat. Chem.* **2013**, *5*, 739. (c) Sánchez-Sánchez, C.; Brüller, S.; Sachdev, H.; Müllen, K.; Krieg, M.; Bettinger, H. F.; Nicolaï, A.; Meunier, V.; Talirz, L.; Fasel, R.; Ruffieux, P. *ACS Nano* **2015**, *9*, 9228.

Table of Contents Graphic